- Technical paper -

ANALYTICAL STUDY ON INFLUENCE OF MORTAR-AGGREGATE INTERFACE CHARACTER ON CONCRETE STRENGTH BY RBSM

Kohei NAGAI[*1], Yasuhiko SATO[*2] and Tamon UEDA[*2]

ABSTRACT: Concrete is a heterogeneity material consisting of mortar and aggregate in meso scale. Evaluation of fracture process in this scale is useful to clarify the material characteristics of concrete. However, analytical approach in this scale has not been carried out enough yet. And in meso scale, mortar-aggregate interface is the weakest part in concrete so that it is considered that its material property affect the strength of concrete. In this study, influence of interface characteristic on concrete strength is simulated by 3D Rigid Body Spring Analysis. The reduction of strength of model due to the deterioration of interface character can be simulated qualitatively.
KEYWORDS: 3D RBSM, meso scale analysis, mortar-aggregate interface, Voronoi geometry

1. INTRODUCTION

Study on concrete in meso scale in which concrete is consisting of mortar and aggregate is useful for the precise evaluation of its material characteristics that are affected by those of components. Many experimental researches were conducted on fracture mechanism in meso scale in the past. In these researches, fracture propagation from the interface between mortar and aggregate to the mortar part is observed in the failure process of concrete [1][2]. And the effect of material characteristics of interface on concrete strength is examined and the significant reduction of compressive strength of concrete is observed when the bond of interface is cut by soft layer coating of aggregate [3][4]. Though analytical approaches in meso scale have been conducted in these years [5], influence of bond characteristic on concrete strength has not been examined by analysis yet. In this study, this influence is simulated by three-dimensional Rigid Body Spring Model (RBSM). This analysis method is useful to simulate a discrete behavior like concrete fracture. Analyses of compression test of concrete specimen where shape of the aggregate is sphere are conducted and the reduction ratio of strength is compared with previous experimental results. The authors had developed 3D RBSM analytical system and showed its reliability by the simulations of mortar and concrete failures [6].

2. METHOD OF NUMERICAL ANALYSIS

The RBSM developed by Kawai is one of discrete numerical analysis method [7]. The analytical model is divided into polyhedron elements whose phases are interconnected by springs. Each element has three transitional and three rotational degrees of freedom at the center of gravity. One normal and two shear springs are placed at the centroid of each face (Fig.1). Since cracks initiate and propagate along the boundary face, the element arrangement may affect fracture direction. To avoid formation of cracks in a certain direction, a random geometry is introduced using a three-dimensional Voronoi diagram (Fig.2). The Voronoi diagram is the collection of Voronoi cells. Each cell represents mortar or aggregate element in the analysis.

In the nonlinear analysis, stiffness matrix is constructed by the principle of virtual work [7], and the Modified Newton-Raphson method is employed for the convergence algorithm. When the model does not converge at the given maximum iterative calculation number, analysis proceeds to the next step.

*1 Division of Structural and Geotechnical Engineering, Hokkaido University, M.E., Member of JCI
*2 Division of Structural and Geotechnical Engineering, Hokkaido University, Dr.E, Member of JCI

3. CONSTITUTIVE MODELS [6]

3.1 MORTAR MODEL

In this study, a constitutive model for mortar in meso level is developed because the constitutive model in macro scale cannot be applied to meso scale analysis.

Material characteristics of each component are presented by means of modeling springs. In normal springs, compressive and tensile stresses (σ) are developed. Shear springs develop shear stresses (τ). For the calculation of shear stress, a resultant value of strains generated in two shear springs is adopted as a shear strain in the constitutive model presented in this section.

Elastic modulus of springs are presented as follows,

$$k_n = \frac{(1-\nu_{elem})E_{elem}}{(1-2\nu_{elem})(1+\nu_{elem})}$$
$$k_s = \frac{E_{elem}}{2(1+\nu_{elem})} \qquad (1)$$

where k_n and k_s are the elastic modulus of normal and shear spring, E_{elem} and v_{elem} are the elastic modulus and Poisson's ratio of component for meso level, respectively.

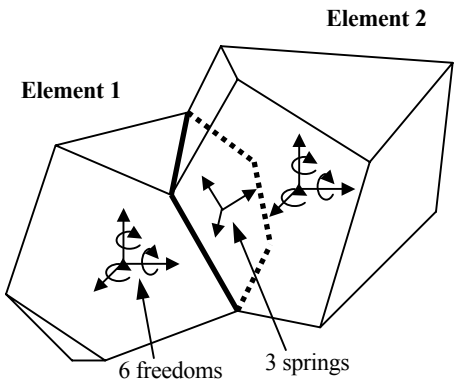

Fig. 1 Mechanical model

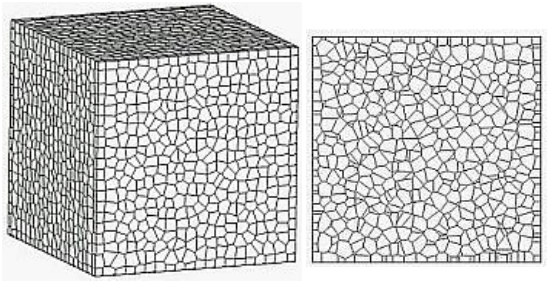

a) 3D view **b) Cross section**

Fig. 2 3D Voronoi geometry

In the analysis, due to the modeling nature for RBSM, values of the material property, which are the material property in meso level, given to the element are different from those of the analyzed object as the macroscopic material property. In this study, the material properties for the element were determined in such a way to give the correct macroscopic properties. For this purpose, the elastic analysis of mortar in compression was carried out. In discrete analysis such as RBSM analysis, shape of elements and element fineness affect the result of analysis [8]. To reduce these effects, small size for element is adopted and element finenesses in all analyses are in almost same level. Volume of each element is about 2.5~3.0mm^3 in this study. In the elastic analyses, the relationship between the macroscopic and mesoscopic Poisson's ratio and the effect of the mesoscopic Poisson's ratio on the macroscopic elastic modulus were examined. From the results, Eq.(2) is adopted for determining the mesoscopic material properties.

$$\nu_{elem} = -237.0\nu^4 + 266.6\nu^3 - 116.1\nu^2 + 24.1\nu - 1.6 \qquad (0.12 \leqq \nu \leqq 0.35)$$
$$E_{elem} = \left(-41.5\nu_{elem}{}^4 + 21.1\nu_{elem}{}^3 - 5.5\nu_{elem}{}^2 + 0.4\nu_{elem} + 1.3\right)E \qquad (2)$$

where E and v are macroscopic elastic modulus and Poisson's ratio of component of analyzed object, respectively.

Only the maximum tensile stress has to be set as a material strength. Actually, mortar itself is not a homogeneous material, which is consisting of sand and paste, even when bleeding effect is ignored. Strength variation in mortar has not been clarified yet. In this study, a normal distribution is assumed for the tensile strength of spring element. The probability density function is as follows (Fig. 3),

$$f(f_{t\,elem}) = \frac{1}{\sqrt{2\pi}} \exp\left\{-\frac{\{3(f_{t\,elem}/f_{t\,average}-1)\}^2}{2}\right\} \qquad \text{,when } f_{t\,elem} < 0 \text{ then, } f_{t\,elem} = 0 \qquad (3)$$

where $f_{t\,elem}$ is distributed tensile strength and $f_{t\,average}$ is average tensile strength of mortar in meso level. The same distribution is given to the elastic modulus. Those distributions affect the macroscopic elastic modulus,

so that the elastic modulus for the element given by Eq.(2) is multiplied by 1.05.

Springs set on element faces act elastic until stresses reach to τ_{max} criterion or tensile strength. The strains and stresses are calculated as follows,

$$\varepsilon = \frac{\Delta n}{h_1 + h_2} \quad , \quad \gamma = \frac{\Delta s}{h_1 + h_2}$$
$$\sigma = k_n \varepsilon \quad , \quad \tau = k_s \gamma \qquad (4)$$

where ε and γ are the strain of normal and shear springs. Δn and Δs are the normal and shear relative displacement of elements those compose springs and h is the length of perpendicular line from the center of gravity of element to the boundary face. Subscripts 1 and 2 represent elements 1 and 2 in Fig.1, respectively.

Constitutive model of normal spring is shown in Fig. 4. In compression zone, it always acts elastic. Fracture happens between elements when spring reaches tensile strength $f_{t\,elem}$, and the normal stress decreases linearly depending on crack width that is the spring elongation. In this study, stress-free crack width w_{max} is set 0.005mm. The linear unloading and reloading path that goes through the origin is introduced to normal spring in tension zone. For shear spring, elasto plastic model is applied as shown in Fig.5 in the range that normal spring dose not have fracture. Value of τ_{max} changes depending on the condition of normal spring and given as follows,

$$\tau_{\max} = \pm\left\{0.08 f_{telem}{}^{2.7}\left(-\sigma + f_{telem}\right)^{0.7} + f_{telem}\right\} \qquad \left(\sigma < f_{telem}\right) \qquad (5)$$

When fracture happens in normal spring, the calculated shear stress is reduced corresponding to the reduction ratio of normal stress. As a result, shear spring cannot carry the stress either when crack width of normal spring reaches w_{max}.

In this study, normal springs in compression only behave elastically and never break nor have softening behavior.

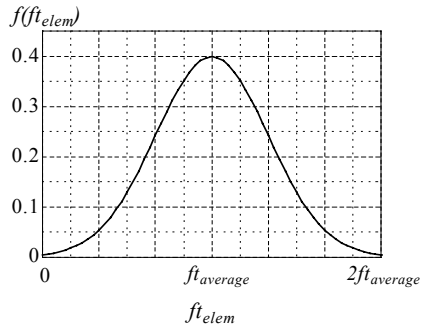

Fig. 3 Distribution of material properties

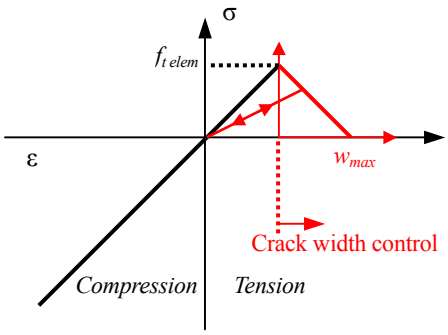

Fig. 4 Model of normal spring

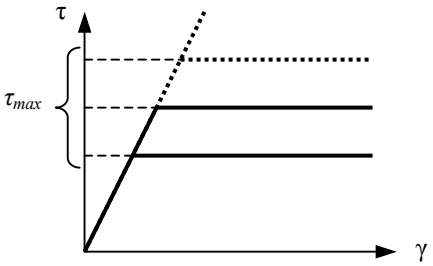

Fig. 5 Model of shear spring

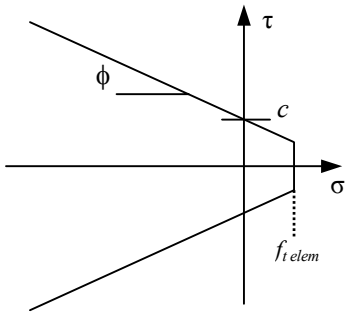

Fig. 6 τ_{max} criterion for interface

3.2 AGGREGATE MODEL

In this study, effect of existence of aggregate in concrete on fracture process is examined. For this purpose, element of aggregate behaves only elastic without fracture in this study. The same equations as Eqs.(1), (2), and (4) are adopted to present the material property of aggregate.

3.3 INTERFACE MODEL

The same stress-strain relationships as Eq.(4) and strength and stiffness distribution as Eq.(3) are adopted for the material properties of the interface between mortar and aggregate. The spring stiffnesses k_n and k_s (Eq.(1)) of the interface are given by a weighted average of the material properties in two elements according to their length of perpendicular line from the center of gravity of element to the boundary face where springs are set. For the interface between mortar and aggregate, the τ_{max} criterion as shown in Eq.(6) and Fig.6 is adopted.

$$\tau_{\max} = \pm(-\sigma \tan\phi + c) \qquad (\text{for } \sigma < f_{telem}) \qquad (6)$$

where ϕ and *c* are material constants. This criterion is based on the failure criterion suggested by Kosaka et al. which is derived from experimental results [4]. After stresses reach the failure criterion, the shear stress (τ) is reduced to τ_{max} which depends on the normal stress (σ) in the range where the normal stress is in compression. In the tension stress range, both normal and shear stresses cannot transfer the stress after the stresses reach the criterion.

4. ANALYSIS

Compression analyses of mortar and concrete specimens are conducted to simulate the influence of interface characteristics. Table 1 shows the parameter of simulated specimens. Totally 5 analyses are carried out in this study where aggregate volume and constitutive model for interface are varied. Two types of constitutive model for interface are applied to the same specimen to examine the influence of interface bond characteristics: (i) the constitutive model developed in this study (see Section 3.3) – With bond; (ii) the constitutive model where only the compressive stress through the normal spring can be transferred and the tensile and shear stresses never be transferred. It means that bond in interface is cut and intends to represent the condition that aggregates are coated by soft layer – Without bond. Table 2 shows the input material properties in the analysis where only the tensile strengths are given as a material strength. Ordinary values are adopted as material properties of mortar and aggregate. To determine the material properties of interface, previous researches are referred and typical values are selected [4][9][10].

Fig. 7 shows the 3D view of simulated specimen of mortar, location of aggregates in the 18% and 34% aggregate specimens and *x*-*y* cross-sections at *z*=37.5mm. Size of the

Table 1 Analytical specimens

Specimen	Aggregate volume	Interface model
Mortar	0%	-
A18%-W	18%	With bond
A18%-W/O	18%	Without bond
A34%-W	34%	With bond
A34%-W/O	34%	Without bond

Table 2 Input material properties

Mortar		
$f_{t\,average}$	Elastic modulus (*E*)	Poisson's ratio (*v*)
4.2 MPa	24,000 MPa	0.18
Aggregate		
Elastic modulus (*E*)	Poisson's ratio (*v*)	
50,000 MPa	0.25	
Interface		
$f_{t\,average}$	c	ϕ
1.6 MPa	2.7 MPa	35°

Table 3 Number of element of analytical specimens

Specimen	Number of element (Aggregate)	Average element size
Mortar	48778 (0)	2.59 mm^3/ element
18% aggregate	48404 (11129)	2.59 mm^3/ element
34% aggregate	45744 (17531)	2.64 mm^3/ element

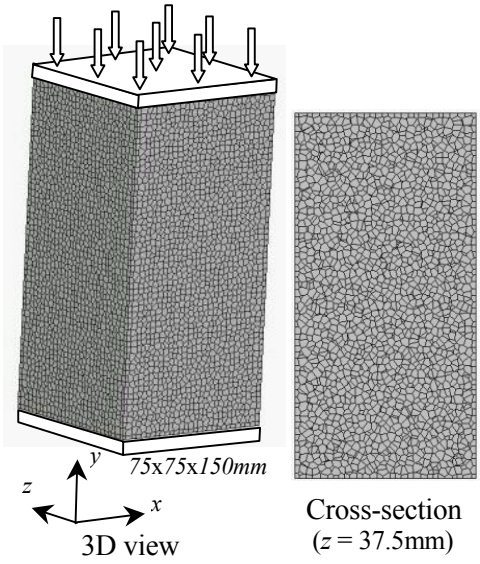

a) Mortar specimen

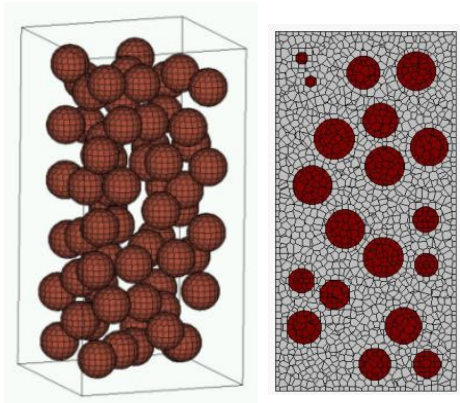

b) 18% aggregate specimen

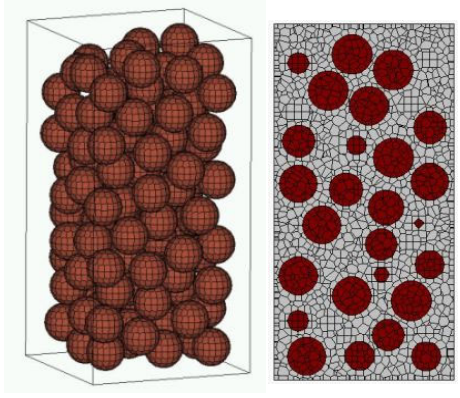

c) 34% aggregate specimen

Fig. 7 Analytical specimens

model is 75x75x150mm and 16.6mm diameter aggregates are introduced randomly. Number of elements and average element size are shown in Table 3. The two types of constitutive model of interface are applied to 18% and 34% specimens in Fig.7 (see Table 1). In the analyses, top and bottom loading boundaries are fixed in lateral direction and the rotations of the boundaries are not allowed.

Fig. 8 shows the predicted stress-strain curves. Simulated result of mortar and the shape of the curves are discussed in the previous study of the authors [6]. Reduction of strengths due to the introduction of aggregates and the eliminating bond are observed. Reduction ratio in the analysis and the experimental result conducted by Christensen et al. [3] are shown in Fig.9. In the experiment, compression tests of mortar and concrete in which marble spheres with 16.6mm diameter weire introduced as aggregates and the aggregates were coated by soft plastic layer in the 'Without bond' specimens were carried out. The values at age of 28days for the concrete are adopted in the graph. Though some conditions are different in the analysis and experiment, the analysis can simulate the reduction of strength qualitatively. Fig. 10 shows the deformation at failure (at axial strain of -2,000μ) of specimen A18%-W. Macroscopic shear crack observed in usual experiment can be simulated and this crack pattern is observed in other concrete analyses in this study. Curves in Fig. 11 show the numbers of faces of interface and mortar whose crack width reach 0.002mm, 0.005mm and 0.03mm in specimens A18%-W and A18%-WO. Horizontal axes show the macroscopic strain of specimens. The macroscopic stresses of the specimens are presented in the graphs. In both specimens, number of crack on interface increases fast and the specimen comes to failure after the rapid increasing of mortar crack. Those facts are same as usual experimental result [1][2]. Crack on interface of specimen A18%-WO increases from significantly lower stress level than that of specimen A18%-W because of the cut of bond (see Fig. 11 a) and c)). This increasing of interface crack causes the much nonlinearity and the strength reduction of specimen A18%-WO. Interface conditions of specimens A18%-W and A18%-WO at axial strain -500μ, -1,000μ and -1,500μ are presented in Fig. 12. Black face shows the cracked face. In both specimens, analysis can simulate the development of the crack band on the side of the aggregates that is observed in experiment

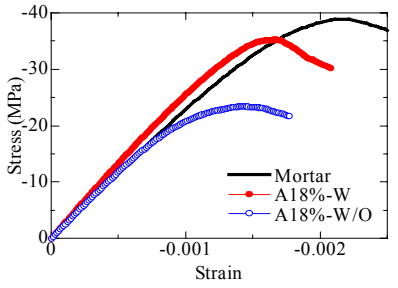

Fig. 8 Predicted stress strain curves

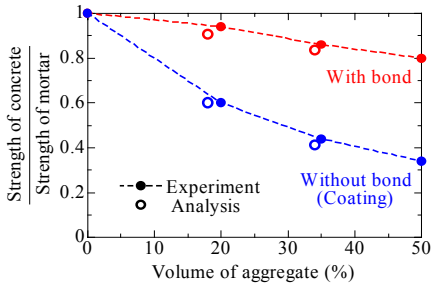

Fig. 9 Strength reduction of concrete

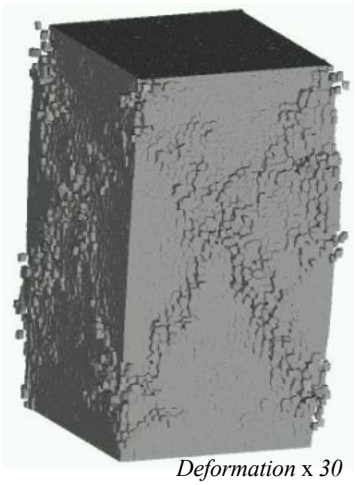

Fig. 10 Deformation at failure (Specimen A18%-W)

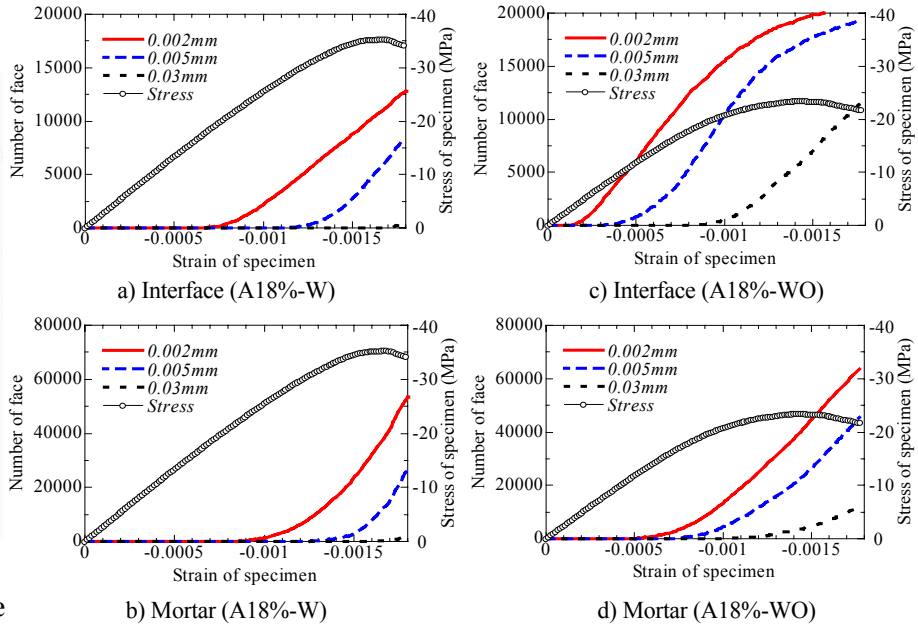

Fig. 11 Number of faces reaching certain crack widths

[4]. As the fact seen in Fig. 11, rapid progress of interface crack in specimen A18%-WO is confirmed in Fig. 12.

Behaviors similar to those specimens A18% series mentioned in this section are observed in A34% series. The strength reduction of A34% series is bigger than that of A18% series (See Fig.8) because the area of interface that is the weakest part in the concrete is larger.

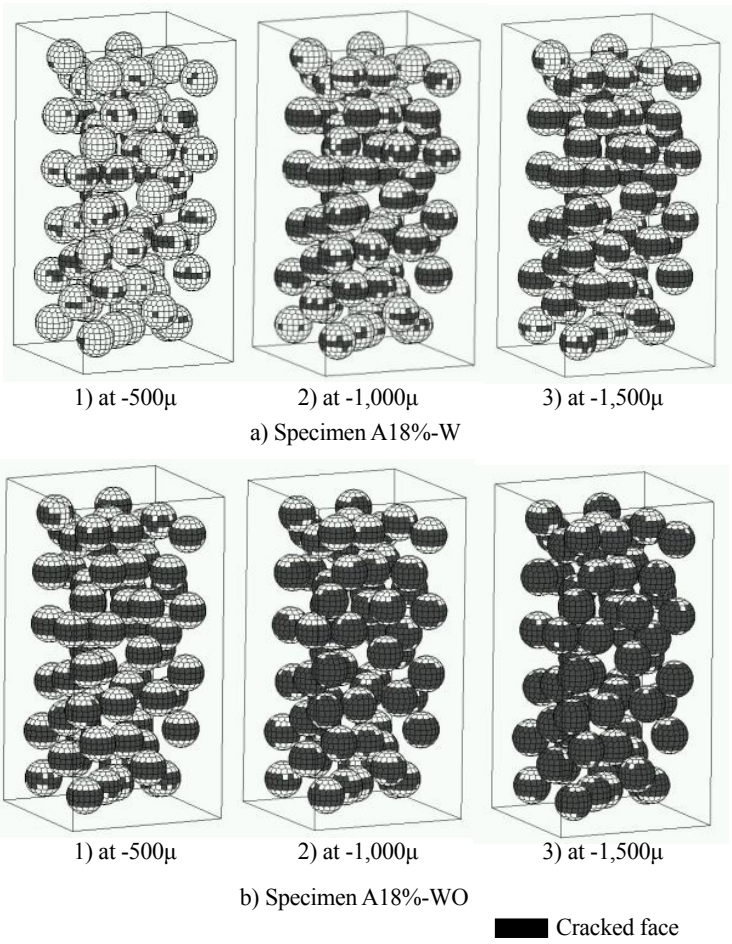

Fig. 12 Progress of cracked interface

5. CONCLUSIONS

The followings are concluded from the analyses of mortar and concrete by 3D RBSM.

(1) Analysis can simulate the reduction of strength in compression due to the introduction of aggregates and the cut of bond well qualitatively.
(2) Macroscopic shear crack patterns are simulated in the analyses of concrete.
(3) In the analysis, interface crack on the side of aggregates in 'Without bond' specimen propagates faster than 'With bond' specimen. This faster propagation causes the reduction of macroscopic strength.

REFERENCES

1. Kato, K., "Microcracks and Physical Properties of Plane Concrete," Proc. of JSCE, JSCE, Vol.188, April 1971, pp.61-72. (in Japanese)
2. Kosaka, Y. and Tanigawa, H, "Effect of Coarse Aggregate on Fracture of Concrete (Part 2)," Proc. of AIJ, AIJ, Vol.231, May 1975, pp.1-11. (in Japanese)
3. Christensen, P.N. and Nielsen, T.P.H., "Modal Deformation of the Effect of Bond Between Coarse Aggregate and Mortar on the Compressive Strength of Concrete," ACI Journal, ACI, Vol.66, Jan. 1969, pp.69-72.
4. Kosaka, Y., Tanigawa, H. and Kawakami, M., "Effect of Coarse Aggregate on Fracture of Concrete (Part 1)," Proc. of AIJ, AIJ, Vol.228, Feb. 1975, pp.1-11. (in Japanese)
5. Asai, M. et al, "Meso-scopic Numerical Analysis of Concrete Structure by a Modified Lattice Model," J. Struct. Mech. Earthquake Eng., JSCE, No.731/I-63, April 2003, pp.19-30.
6. Nagai, K., Sato, Y. and Ueda, T., "Three-dimensional Numerical Simulation of Mortar and Concrete Model Failure in Meso Level by Rigid Body Spring Model," Journal of Structural and Engineering, JSCE, Vol.50A, Mar. 2004, pp.167-178.
7. Kawai, T. and Takeuchi, N., "Discrete Limit Analysis Program, Series of Limit Analysis by Computer 2," Baifukan, 1990. (in Japanese)
8. Nagai, K., "Numerical Simulation of Fracture Process of Concrete Model by Rigid Body Spring Method," Master Thesis submitted to Hokkaido University, 2002.
9. Taylor, M.A. and Broms, B.B., "Shear Bond Strength Between Coarse Aggregate and Cement Paste or Mortar," ACI Journal, ACI, Aug. 1964, pp939-956.
10. Hsu, T.T.C. and Slate, F.O., "Tensile Bond Strength Between Aggregate and Cement Paste or Mortar," ACI Journal, ACI, April 1963, pp.465-485.